https://journals.aps.org/prd/abstract/10.1103/PhysRevD.106.124042

Energy extraction in electrostatic extreme binary black holes

A. Baez[1,*], Nora Breton [1,†], and I. Cabrera-Munguia [2,‡]
[1] *Departamento de Física, Centro de Investigación y de Estudios Avanzados del I. P. N. Apdo. Postal 14-740, Mexico City, Mexico*
[2] *Departamento de Física y Matemáticas, Universidad Autónoma de Ciudad Juárez, 32310 Ciudad Juárez, Chihuahua, México*

Relying on the Penrose process mechanism, we study the possibility of energy extraction from a binary system composed of two extreme electrostatic black holes (BHs) oppositely charged, separated by a strut described by Bonnor's metric (BM). We determined and plotted the generalized ergosphere that surrounds only one of the BH. We demonstrate the existence of non closed orbits of negative energy outside the event horizon; these orbits allow the possibility of energy extraction by particle disintegration from a system described by the BM. Besides we prove that the extraction process can occur when a charged test particle and the BH have opposite charges; also, we analyzed the efficiency of the process.

PACS numbers:

I. INTRODUCTION

The Kerr metric is a stationary solution of Einstein's field equation that gives the more general description of a rotating BH [1–3]; this metric possesses an interesting region called the ergosphere, delimited by the stationary limit surface and the outer event horizon. When a particle reaches the esgosphere a timelike trajectory becomes spacelike, and a spacelike trajectory becomes timelike and particles inside of the ergosphere can have negative energy. However, the particle can yet avoid enter the event horizon and can escape back to infinity.

The Penrose process is a mechanism proposed by Penrose and Floyd [4] for extracting energy from a rotating BH taking advantage of the fact that test particles inside the ergosphere can have negative energy states. It consists of a particle that reaches the ergosphere and at some point it disintegrates into two fragments, one of the fragments is trapped within the ergosphere with negative energy and the other one escapes back to infinity with more energy than the one of the incident particle; by conservation of energy then rotating energy through angular momentum has been extracted. However, the ergosphere is a characteristic region of stationary solutions, then by means of the Penrose process it is, in principle, impossible to extract energy from a static BH. However, for electrostatic BHs it is possible to define a region where charged test particles can have negative energy [5, 6].

Although the Penrose process applied to a single particle might seem unfeasible to carry out, it is possible to establish relations between the Penrose process and some astrophysical observations. For instance, the collisional Penrose process might eventually eliminate dark energy particles in the vicinity of a supermassive BH once the multiple particles that scatter inside the ergosphere achieve an arbitrarily high center of mass energy [7]. On the other hand, the influence of an external magnetic field surrounding a rotating BH can form accretion disks of charged ionized matter [8] and this may be related to high-frequency oscillations noticed in microquasars, galactic nuclei, or even the magnetic Penrose process itself [9] where ultra high-energy particles around rotating magnetized BHs are created [10, 11]. Moreover, the radiative Penrose process is connected to synchrotron radiation of charged particles moving within the ergosphere of a magnetized BH, where such a process considers a special type of radiated photons having negative energy relative to a distant observer [12, 13]. In addition, recent numerical studies on plasmas and jets suggest the main role of negative energy particles and the Penrose process in the total flux coming from the BH jets [14]. Finally, the electromagnetic Penrose process [15–20] allows events of high energy emission in contrast with the efficiency of 20.7% of the well-known Penrose process due only to the rotation of a Kerr BH.

The present paper aims to investigate energy extraction via the Penrose process in a BH binary system. In [21] the energy extraction is analyzed for the Majumdar-Papapetrou (MP) binary metric [22–24], which is an exact solution of the Einstein-Maxwell equations describing two static charged BHs whose charges equal their masses, $Q_i = M_i$, $i = 1, 2$. Therefore, in the MP binary metric, the BHs remain in neutral equilibrium since their mutual gravitational attraction compensates their mutual electric repulsion no matter how far apart the sources are. Our purpose is to use the method developed in [5, 6] to determine negative energy states for charged test particles and prove that by means of the Penrose process is possible the energy extraction in a binary system composed of two electrostatic oppositely charged BHs described by Bonnor's metric (BM) [25, 26], where now the gravitational attraction does not counterbalance the electrical repulsion, and therefore, a conical singularity arises [27, 28] in between the sources. In particular we study the generalized ergosphere, its dependence on charged test particle and how the energy extraction efficiency is

*jbaez@fis.cinvestav.mx
†nora@fis.cinvestav.mx
‡icabreramunguia@gmail.com

affected by the presence of a BH companion with opposite charge.

Our paper is organized as follows. In Sec. II A, we introduce the spacetime described by the BM and derive the motion equations for charged massive test particles in a static and axisymmetric spacetime. In Sec. II B the generalized ergosphere and the existence of negative orbits is analyzed. In Sec. III the Penrose process is described and the conservation equations are presented (mass, charge, energy, linear momentum and angular momentum). In Sec. IV the constrictions over the parameters and the maximum efficiency of the process are presented and in the last section conclusions are given.

II. BONNOR'S BINARY BH

Bonnor's metric (BM) [25, 26] is a static solution of Einstein-Maxwell equations that describes a two-body system composed of two electrostatic BHs, separated by a strut [27, 28], which is a line source of pressure that produces a conical singularity (angle's deficit); the strut keeps apart the sources from overlapping with each other. The BM can be derived from the general double Reissner-Nordström spacetime [29] as a particular extreme limit, in this sense the BHs of the BM are called extreme. In this metric, the BH charges, Q_1 and Q_2, are opposite in sign and for two BHs of masses M_1 and M_2 separated by a distance R along the z-axis, are given by [26]

$$Q_1 = M_1\sqrt{\frac{(R+M_2)^2 - M_1^2}{(R-M_2)^2 - M_1^2}},$$
$$Q_2 = -M_2\sqrt{\frac{(R+M_1)^2 - M_2^2}{(R-M_1)^2 - M_2^2}}, \tag{1}$$

the electric charges and masses fulfill the condition $|Q_i| > M_i$, $i = 1, 2$.

The stationary axisymmetric metric in Weyl's cylindrical coordinates (t, ρ, z, ϕ) is the Papapetrou metric [23] given by

$$ds^2 = f^{-1}\left[e^{2\gamma}(d\rho^2 + dz^2) + \rho^2 d\phi^2\right] - f(dt - \omega d\phi)^2, \tag{2}$$

where for a static solution $\omega = 0$. The binary BH BM corresponds to the metric functions

$$f = \left(\frac{1}{1+g_1} + \frac{1}{1+g_2} - 1\right)^2, \qquad e^{2\gamma} = \left(\frac{(1-g_1 g_2)g_+ g_-}{4d^2}\right)^4,$$
$$g_1 = \frac{(1+d)M_1 - (1-d)M_2}{(1+d)r_- - (1-d)r_+}, \quad g_2 = \frac{(1+d)M_2 - (1-d)M_1}{(1+d)r_+ - (1-d)r_-}, \qquad d = \sqrt{\frac{R^2 - (M_1 - M_2)^2}{R^2 - (M_1 + M_2)^2}}$$
$$g_+ = 1 + d - (1-d)\frac{r_+}{r_-}, \qquad g_- = 1 + d - (1-d)\frac{r_-}{r_+}, \qquad r_\pm = \sqrt{\rho^2 + (z \pm R/2)^2}. \tag{3}$$

In Weyl's cylindrical coordinates the BHs and their horizons are represented by points at the z-axis ($\rho = 0, z = \pm R/2$). The independent parameters of the BM (2)-(3) are M_1, M_2 and R while the electric potential A_μ is given by

$$A_\mu = (A_t, A_\rho, A_\phi, A_z) = \left(\frac{1}{1+g_1} - \frac{1}{1+g_2}, 0, 0, 0\right). \tag{4}$$

The interaction force associated with the strut between the BHs is given by [30]

$$\mathcal{F} = \frac{2M_1M_2}{R^2 - (M_1+M_2)^2}\left(1 + \frac{2M_1M_2}{R^2 - (M_1+M_2)^2}\right), \tag{5}$$

and because the masses and distance satisfy the inequality $M_1 + M_2 < R$, only attractive scenarios will be allowed and then the force of the strut is positive $\mathcal{F} > 0$. On the other hand, since the BM is static, the spacetime does not possess an ergosphere in the usual sense where the timelike Killing vector becomes spacelike, as a consequence the energy associated to geodesic motion of neutral particles is always positive, i.e., the energy extraction is not possible. However, charged particles can interact with charged BHs via Lorentz forces. According to the ideas proposed by Denardo-Ruffini [5] for a single charged BH and Sanches-Richartz for a BH binary [21], we can define a particular region where negative energy trajectories and energy extraction are, in principle, possible. In what follows we study the motion of charged particles in the BM that is a binary BH with opposite charges, and analyze the energy extraction.

A. Motion of charged particles

The motion equations for a test particle with charge-mass ratio μ in a spacetime characterized by the metric $g_{\mu\nu}$ and interacting with the electric potential A_μ, can be obtained from the Euler-Lagrange equations with the

Lagrangian

$$\mathcal{L} = \frac{1}{2} g_{\mu\nu} \dot{x}^\mu \dot{x}^\mu + \mu A_\alpha \dot{x}^\alpha, \tag{6}$$

where the dot means derivative with respect to an affine parameter. In terms of the metric coefficients in Eq. (2), the Lagrangian is

$$\mathcal{L} = \frac{1}{2}\left(f^{-1}\left(e^{2\gamma}(\dot{\rho}^2+\dot{z}^2)+\rho^2\dot{\phi}^2\right) - f\dot{t}^2\right) + \mu A_t \dot{t}, \tag{7}$$

which does not depend explicitly on the coordinates t and ϕ. Then we can identify two motion constants of the test particle: its energy E and angular momentum L per unit mass, as measured by observers at infinity, given by

$$\begin{aligned} E &= -\frac{\partial \mathcal{L}}{\partial \dot{t}} = f\dot{t} - \mu A_t, \\ L &= \frac{\partial \mathcal{L}}{\partial \dot{\phi}} = f^{-1}\rho^2\dot{\phi}, \end{aligned} \tag{8}$$

where after solving for $\dot{\phi}$ and $\dot{t}$, and substituting the result into Eq. (7), we obtain the motion equations for ρ and z coordinates, via the Euler-Lagrange equations, as

$$\begin{aligned} \ddot{\rho} - \frac{fe^{-2\gamma}}{2}\frac{\partial}{\partial\rho}\left(\frac{(E+\mu A_t)^2}{f} - \frac{fL^2}{\rho^2}\right) + \left(\frac{\dot{z}^2-\dot{\rho}^2}{2}\right)\frac{\partial}{\partial\rho}\left(\ln\left(fe^{-2\gamma}\right)\right) - \dot{\rho}\dot{z}\frac{\partial}{\partial z}\left(\ln\left(fe^{-2\gamma}\right)\right) = 0, \\ \ddot{z} - \frac{fe^{-2\gamma}}{2}\frac{\partial}{\partial z}\left(\frac{(E+\mu A_t)^2}{f} - \frac{fL^2}{\rho^2}\right) + \left(\frac{\dot{\rho}^2-\dot{z}^2}{2}\right)\frac{\partial}{\partial z}\left(\ln\left(fe^{-2\gamma}\right)\right) - \dot{\rho}\dot{z}\frac{\partial}{\partial \rho}\left(\ln\left(fe^{-2\gamma}\right)\right) = 0. \end{aligned} \tag{9}$$

It is worth mentioning that the motion equations for ρ and z, in terms of the metric (2) are given in [31] for neutral test particles. On the other hand, an explicit expression for the energy E is obtained by plugging the constants of motion (8) into the normalization condition of the four velocity $\dot{x}^\mu \dot{x}_\mu = -1$,

$$E = -\mu A_t \pm \sqrt{e^{2\gamma}\left(\dot{\rho}^2+\dot{z}^2\right) + \frac{L^2 f^2}{\rho^2} + f}, \tag{10}$$

where the positive root is taken for a positive energy at infinity when $\mu = 0$ [6]. After some straightforward algebra, Eq. (10) can be expressed as

$$\dot{\rho}^2 + \dot{z}^2 = E_{\text{eff}}^2(\rho,z) - V_{\text{eff}}(\rho,z), \tag{11}$$

where

$$\begin{aligned} E_{\text{eff}}^2(\rho,z) &= \frac{\left(E+\mu A_t\right)^2}{e^{2\gamma}}, \\ V_{\text{eff}}(\rho,z) &= \frac{1}{e^{2\gamma}}\left(\frac{L^2 f^2}{\rho^2} + f\right). \end{aligned} \tag{12}$$

These expressions are subject to the constraints:

$$E_{\text{eff}}(\rho,z) \geq 0, \qquad E_{\text{eff}}^2(\rho,z) \geq V_{\text{eff}}(\rho,z). \tag{13}$$

The system of equations (9) fully describes the motion of a charged test particle in a static and axisymmetric spacetime; this set of equations can be numerically solved once the appropriate initial conditions are chosen. In order to solve this system of equations, the values for the energy E, angular momentum L, and initial values for ρ, z, and $\dot{z}$ should be given; the initial value for $\dot{\rho}$ is determined from Eq. (10). With these initial values Eqs. (9) can be solved for $\rho(\lambda)$ and $z(\lambda)$ with λ being the affine parameter; the full description of the motion of a test particle is obtained when the set of Eqs. (8) is solved using $\rho(\lambda)$ and $z(\lambda)$.

B. Generalized ergosphere

From the expression (10), we know that the energy is determined by the angular momentum L, charge-mass ratio μ, electric potential A_t and the coordinates and velocities: ρ, z, $\dot{\rho}$ and $\dot{z}$ at a specific time. In order to know if there are test particles with negative energy we consider the minimun energy that it could have with a fixed μ and position (ρ, z); this is the energy associated with test particles at rest. Replacing $\dot{\rho} = 0$, $\dot{z} = 0$, and $L = 0$ in (10), we get

$$E_{\text{min}} = -\mu A_t + \sqrt{f}, \tag{14}$$

since $\sqrt{f} \geq 0$, then the existence of test particles with negative energies is defined by the term $-\mu A_t$. In order that $E_{\text{min}} < 0$, $\mu A_t > 0$. Hence we need to determine the sign of A_t given by,

$$A_t = \frac{1}{1+g_1} - \frac{1}{1+g_2}. \tag{15}$$

Using the explicit form of g_1 and g_2 in Eq. (3) one can easily verify that the sign of A_t is different if (ρ, z) are inside or outside the circle delimited by

$$\bar{\rho}^2 + \left(\bar{z} + \frac{1}{2}\left(\frac{1+M_R^2}{1-M_R^2}\right)\right)^2 = \left(\frac{M_R}{1-M_R^2}\right)^2, \tag{16}$$

where $\bar{\rho} = \rho/R$, $\bar{z} = z/R$ and $M_R = M_2/M_1$. Note that this region encircles the smaller mass. We distinguish

two scenarios:
i) $M_1 > M_2$, then $0 < M_R < 1$, $A_t > 0$ inside the circle in (16), and $A_t < 0$ outside.
ii) $M_2 > M_1$, then $1 < M_R$, $A_t < 0$ inside the circle in (16), and $A_t > 0$ outside. The sketch of both regions is shown in Fig.1.

When the values of M_1 and M_2 are exchanged the sketch corresponding to Fig. 1, is rotated about the $z = 0$ plane; then, without loss of generality, we shall consider only the case $M_1 > M_2$.

In order for $E_{min} < 0$ the sign of μ should be the same than the sign of A_t. In contrast with the MP metric, analyzed in [21], where the two BH charges are positive and then energy can be extracted only by negatively charged test particles, for the BM there exist negative energies for both, positive and negative, charged test particles. On the other hand, with the condition $E_{min} < 0$, Eq. (14) can be written as

$$\bar{\rho}^2 + \bar{z}^2 + \frac{2\mu\left(\bar{M}_1\bar{r}_+ - \bar{M}_2\bar{r}_-\right)\bar{d}}{\bar{d}^2 - 1} + \frac{\bar{d}^2 + 1}{\bar{d}^2 - 1}\bar{r}_+\bar{r}_- < \frac{1}{4}, \quad (17)$$

where $\bar{r}_\pm = r_\pm/R$, $\bar{M}_{1,2} = M_{1,2}/R$ and $\bar{d} = \sqrt{\left(1 - (\bar{M}_1 - \bar{M}_2)^2\right) / \left(1 - (\bar{M}_1 + \bar{M}_2)^2\right)}$ are dimensionless quantities restricted by $\left(\bar{M}_1 + \bar{M}_2\right) < 1$. Recall that $(\bar{\rho}, \bar{z})$ are the coordinates of the initial particle, then (17) restricts the position of the initially at rest particle. Note that this reparametrization is equivalent to fix $R = 1$. The inequality (17) determines the generalized ergosphere on the BM. The sketches of the ergosphere for $\mu > 0$ and $\mu < 0$ are shown in Fig. 2; the charged test particle can have negative energy in the region encircling the BH with opposite charge. For particles with $\mu < 0$ the generalized ergosphere surrounds the upper source Fig. 2.a-2.e. If $|\mu|$ is sufficiently large the generalized ergosphere would surround the region delimited by (16) without including it. On the other hand, for particles $\mu > 0$ the generalized ergosphere surrounds the bottom source, Fig. 2.f-2.h; and if $|\mu|$ is sufficiently large the generalized ergosphere is delimited by (16).

From 2 we see that the generalized ergosphere depends on the parameters μ, M_1 and M_2, i.e., not only on the spacetime geometry but also on the charge of the test particle via μ. The minimum energy per unit mass at a given point inside the ergosphere also depends on μ and one the masses of the BHs. To illustrate this, the energy levels of the ergosphere are shown in Fig. 3 for different values of M_1, M_2 for charge-mass ratio μ positive and negative. One can see that in general the shape of the ergosphere does not change and the magnitude of the energy levels is larger as the test particle gets closer to the BH oppositely charged.

C. Negative energy trajectories

The negative energy trajectories of the charged test particles in the BM are confined inside the ergosphere defined by (17) and this trajectory ends into one of the BHs.

We shall describe two classes of orbits around the BH binary described by BM. The first class of trajectories are orbits with angular momentum $L = 0$; this condition implies that the trajectories are confined to a meridional plane, i.e., a plane with ϕ constant; for simplicity we take $\phi = 0$. Fixing the parameters M_1, M_2, μ and R, and given a set of initial conditions $\rho(0)$, $z(0)$ and $\dot{z}(0)$ we can calculate $\dot{\rho}(\lambda)$ and solve the motion equations (9). In Fig. 4 we show some examples of trajectories of particles with negative energy that are confined inside the generalized ergosphere. Fig. 4.a exhibits three trajectories for $\mu = -5$ and Fig. 4.b exhibits three trajectories for $\mu = 20$. Note in these trajectories one of them ends at one of the BHs.
The second class of orbits is a projection of geodesics in the plane $z = 0$; in general, a particle that initially is located at $z = 0$ is not restricted to maintain its movement in this plane. Since the generalized ergosphere for positive μ is always contained in the circle depicted by Eq. (16) (see Figs. 2.f-2.h), then the ergosphere does not reach the plane $z = 0$; then we only show the movement for negative μ. Setting $z = 0$ in motion Eqs. (9) and energy condition Eq. (11), the motion in the $z = 0$ plane is constrained to the region $E^2_{\text{eff}}(\rho, 0) \geq V_{\text{eff}}(\rho, 0)$ where the equality is satisfied for circular orbits. Fig. 5 shows the energy and effective potential for BM at the $z = 0$ plane. The corresponding trajectory is also shown in Fig. 5.

III. PENROSE PROCESS

Now we investigate the possibility of energy extraction from the binary BM. Considering Penrose process developed in [4], extended for RN BHs [5] and lately applied to MP binary BH [21], we addressed the Penrose process for the BM. It consists in sending a charged particle towards the binary BH; at some point once inside the generalized ergosphere, the particle breaks up into two fragments, one of them escapes to infinity with more energy than the initial one while the other remains inside the ergosphere until it falls into one of the event horizons. We denote the initial particle with subscript 0, the particle that falls into the BH with subscript 1 and the particle that escapes with subscript 2. We consider that the incident particle follows the trajectory $T_{(0)}$, which starts outside the ergosphere and ends inside it, at the break-up point (ρ_*, ϕ_*, z_*). From the break-up point emerge two trajectories, labeled $T_{(1)}$ which corresponds to the particle with negative energy ($E_{(1)} < 0$) that remains inside the ergosphere and the trajectory $T_{(2)}$ corresponds to the particle escaping to infinity. The $T_{(i)}$ trajectories are timelike paths $x^\mu_i(\lambda)$ parametrized by the proper time λ. We denote as $m_{(i)}$, $\mu_{(i)}$, $E_{(i)}$, $L_{(i)}$, and $P^\mu_{(i)}$, the mass, the charge-mass ratio, the energy per unit mass, the angular momentum per unit mass (with respect to the z axis) and the four momentum of the i-particle, re-

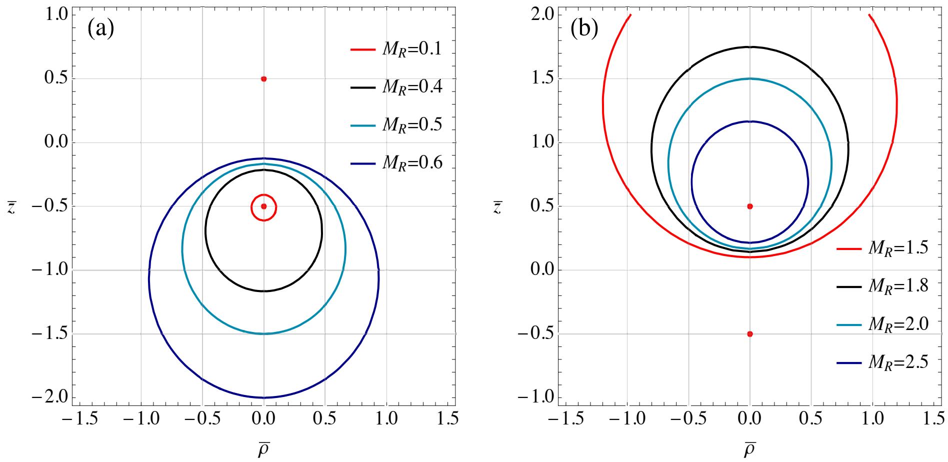

FIG. 1: The sign of the electric potential, A_t depends on the chosen (ρ, z); (a) If $M_1 > M_2$, $0 < M_R < 1$ then A_t is positive inside the circle that surrounds the bottom source, and negative outside. (b) On the other hand, if $M_1 < M_2$, $M_R > 1$ then A_t is negative inside the circle that surrounds the upper source, and positive outside.

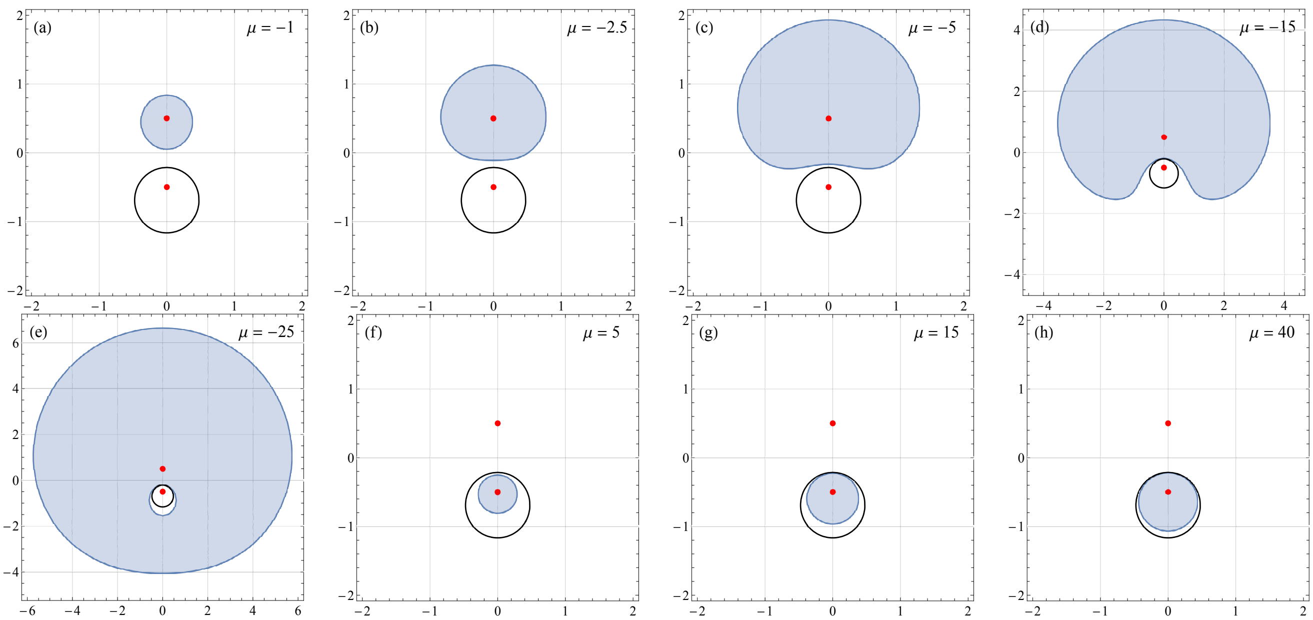

FIG. 2: It is shown the $\phi = 0$ (meridional) plane section of the generalized esgosphere (shaded surface) for different values of μ and fixed values of $\bar{M}_1$ and $\bar{M}_2$. The black circumference represents Eq. (16) and the dots symbolize the BHs. The shadow regions in (a)-(e) represent the ergosphere for $\mu < 0$; note that the ergosphere surrounds only the upper positively charged source and excludes the region delimited by the black circumference. Inside the black circumference $\mu A_t < 0$ and $E_{min} > 0$. On the other hand, the shadow regions in (f)-(h) represent the ergosphere for $\mu > 0$ that is surrounding the bottom (negatively charged) source. For an arbitrarily large value of $|\mu|$ the ergosphere tends to occupy the space inside the black circumference.

spectively. The quantities that characterize each particle should fulfill charge, energy and momentum conservation equations. From the charge conservation we have,

$$\mu_{(0)} m_{(0)} = \mu_{(1)} m_{(1)} + \mu_{(2)} m_{(2)}. \tag{18}$$

On the other hand, if we consider that at the break-up point the four momentum is conserved,

$$P^{\nu}_{(0)} = P^{\nu}_{(1)} + P^{\nu}_{(2)}. \tag{19}$$

From the temporal component in Eq. (19) we have the conservation of the total energy, i.e.

$$E_{(0)} m_{(0)} = E_{(1)} m_{(1)} + E_{(2)} m_{(2)}, \tag{20}$$

while the spatial components of Eq. (19) are the conservations of linear momenta in each component, i.e.,

$$\begin{aligned} m_{(0)} \dot{\rho}_{(0)} &= m_{(1)} \dot{\rho}_{(1)} + m_{(2)} \dot{\rho}_{(2)}, \\ m_{(0)} \dot{z}_{(0)} &= m_{(1)} \dot{z}_{(1)} + m_{(2)} \dot{z}_{(2)}, \end{aligned} \tag{21}$$

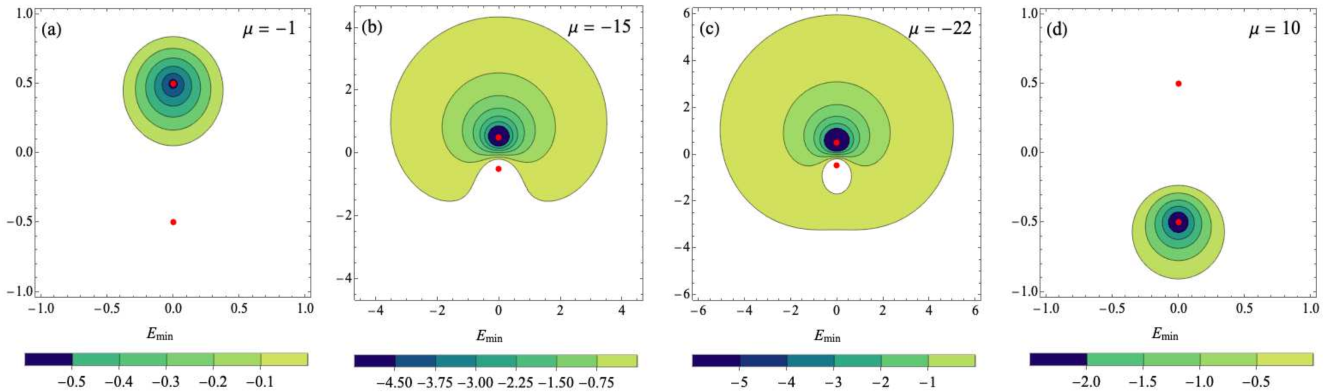

FIG. 3: Energy levels in the generalized ergosphere of the BM are illustrated with $R = 1$, $M_1 = 0.5$, $M_2 = 0.2$ and selected values of μ. The color bar represents E_{min}. The dots indicate the location of the BHs. The horizontal and vertical axes are ρ and z, respectively.

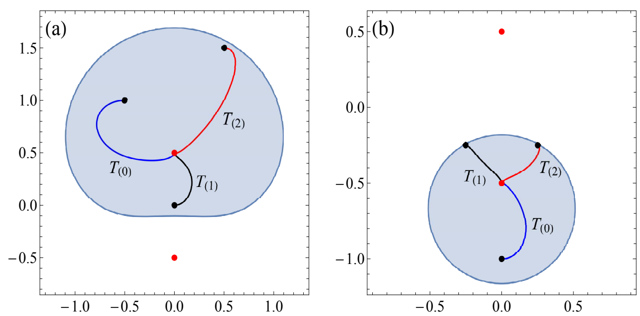

FIG. 4: (a) Examples of trajectories for particle with charge-mass ratio $\mu = -5$; the other parameters are specified for each trajectory. $T_{(0)}$: $E = -0.1$, $\rho(0) = -1/2$, $z(0) = 1$, $\dot{\rho}(0) = -0.73758$ and $\dot{z}(0) = 0$. $T_{(1)}$: $E = -0.00001$, $\rho(0) = 0$, $z(0) = 0$, $\dot{\rho}(0) = 1.32396$ and $\dot{z}(0) = 0$. $T_{(2)}$: $E = -0.0001$, $\rho(0) = 1/2$, $z(0) = 3/2$, $\dot{\rho}(0) = 0.250857$ and $\dot{z}(0) = 0$. (b) Examples of trajectories for particle with charge-mass ratio $\mu = 20$; the other parameters are specified for each trajectory. $T_{(0)}$: $E = -0.002$, $\rho(0) = 0$, $z(0) = -1$, $\dot{\rho}(0) = 0.998144$ and $\dot{z}(0) = 0$. $T_{(1)}$: $E = -0.002$, $\rho(0) = -1/4$, $z(0) = -1/4$, $\dot{\rho}(0) = 0.423686$ and $\dot{z}(0) = 0$. $T_{(2)}$: $E = -0.002$, $\rho(0) = 1/4$, $z(0) = -1/4$, $\dot{\rho}(0) = 0.423686$ and $\dot{z}(0) = 0$.

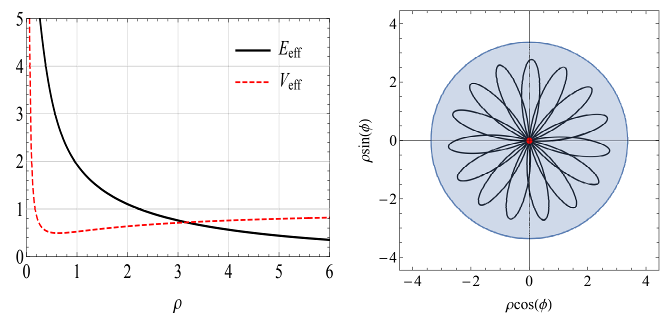

FIG. 5: Left: Effective energy (black curve) and effective potential (red dashed curve) for $L = 0.71$, $E = -0.15$, $M_1 = 0.5$, $M_2 = 0.2$ and $R = 1$. Right: example of a trajectory of negative energy at the $z = 0$ plane with initial conditions $\rho(0) = 2.19858$, $\phi(0) = 0$ and $\dot{\rho}(0) = 1.22395$. The blue circle corresponds to the generalized ergosphere.

where the derivatives $\dot{\rho}_{(i)}$ and $\dot{z}_{(i)}$ should be evaluated at the break-up point. Besides, the conservation of angular momentum is

$$m_{(0)}L_{(0)} = m_{(1)}L_{(1)} + m_{(2)}L_{(2)}. \tag{22}$$

Finally there is an additional restriction on the masses $m_{(i)}$; squaring the four momentum (19) and using the condition $P^{\mu}_{(1)}P_{\mu(2)}$ (future-pointing timelike vectors)[15, 21], we have,

$$m^2_{(1)} + m^2_{(2)} < m^2_{(0)}. \tag{23}$$

IV. ENERGY EXTRACTION EFFICIENCY

The efficiency η of the Penrose process can be defined as the ratio between the energy output (energy of the outgoing particle) and the energy input (energy of the incident particle). From (20), we have

$$\eta = \frac{E_{(2)}m_{(2))} - E_{(0)}m_{(0)}}{E_{(0)}m_{(0)}} = -\frac{E_{(1)}m_{(1)}}{E_{(0)}m_{(0)}}. \tag{24}$$

In order to maximize the efficiency of the process we need to make $E_{(1)}$ as large as possible and $E_{(0)}$ as small as possible. On the other hand the mass of the negative energy fragment $m_{(1)}$ should be as massive as possible in comparison with $m_{(0)}$. In order to deduce the values of the parameters that maximizes the efficiency we choose particular values for BM parameters M_1, M_2, R, the break-up point coordinates (ρ_*, z_*), and the charge-mass ratio $\mu_{(1)}$. With these considerations we analyze how much energy can be extracted from the BM binary BH.

A. Maximum efficiency

The minimum energy of the incident particle coming from infinity, according to Eq. (10) is $E_{(0)} = 1$ and it corresponds to the particle having zero kinetic energy at infinity. On the other hand, with the purpose of maximizing the efficiency, the absolute value of the energy $E_{(1)}$ should be as large as possible, this occurs when the particle $m_{(1)}$ is initially at rest. Recalling that $E_{(1)} < 0$, at the break-up point we set

$$\dot{\rho}_{(1)} = \dot{z}_{(1)} = \dot{\phi}_{(1)} = 0, \tag{25}$$

hence, the angular momentum per unit mass and energy per unit mass are, respectively, $L_{(1)} = 0$ and

$$E_{(1)}(\rho_*, z_*) = E^{min}_{(1)}(\rho_*, z_*) = -\mu_{(1)}A_{t*} + \sqrt{f_*}, \tag{26}$$

where A_{t*} and f_* are evaluated at the break-up point (ρ_*, z_*). Now, we determine the restrictions over the masses $m_{(0)}$, $m_{(1)}$ and $m_{(2)}$. From the linear momentum conservation Eqs. (21), we have

$$\begin{aligned} m^2_{(2)} =& m^2_{(0)}\frac{\dot{\rho}^2_{(0)} + \dot{z}^2_{(0)}}{\dot{\rho}^2_{(2)} + \dot{z}^2_{(2)}} + m^2_{(1)}\frac{\dot{\rho}^2_{(1)} + \dot{z}^2_{(1)}}{\dot{\rho}^2_{(2)} + \dot{z}^2_{(2)}} \\ &- 2m_{(0)}m_{(1)}\frac{\dot{\rho}_{(0)}\dot{\rho}_{(1)} + \dot{z}_{(0)}\dot{z}_{(1)}}{\dot{\rho}^2_{(2)} + \dot{z}^2_{(2)}}. \end{aligned} \tag{27}$$

If we consider the condition given by Eq. (25), and using $\left(\dot{\rho}^2_{(i)} + \dot{z}^2_{(i)}\right)$ from Eq. (11), substituting in Eq. (27), yields

$$m_{(2)} = \sqrt{m^2_{(0)} - 2m_{(0)}m_{(1)}\alpha_{(0)} + m^2_{(1)}}, \tag{28}$$

where

$$\alpha_{(0)} = \frac{1 + A_{t*}\mu_{(0)}}{\sqrt{f_*}}, \tag{29}$$

where f_* and A_{t*} are evaluated at the break-up point. $\alpha_{(0)}$ can be written as $\alpha_{(0)} = E_{\mathrm{eff}(0)}\sqrt{V_{\mathrm{eff}(0)}}$ using Eqs. (12) for an initially at rest particle at infinity ($E_{(0)} = 1$, $L = 0$), hence $\alpha_{(0)}$ is always positive. The MP case is recovered with $f_* \to 1/U^2_*$ and $A_{t*} \to 1/U_* - 1$ where U_* is the interaction potential for MP binary BH [21].

From the inequality (23), squaring (28), and using the fact that the masses are positive, we obtain

$$0 < m_{(1)} < m_{(0)}\left(\alpha_{(0)} - \sqrt{\alpha^2_{(0)} - 1}\right). \tag{30}$$

Where a necessary condition for the masses to have real values is $\alpha^2_{(0)} \geq 1$, namely,

$$\alpha_{(0)} = \frac{1 + A_{t*}\mu_{(0)}}{\sqrt{f_*}} \geq 1, \tag{31}$$

then the values of $\mu_{(0)}$ depend on the location of the break-up point, since A_{t*} is positive/negative, depending if it is evaluated inside/outside of the region defined by Eq. (16). For the case where the break-up point occurs inside Eq. (16), μ_0 is constrained by

$$\mu_{(0)} \geq \frac{\sqrt{f_*} - 1}{A_{t*}}. \tag{32}$$

Have in mind that the extraction process occurs in this region if $\mu_{(0)}$ is positive and the BH is negatively charged. On the other hand, if the break-up point occurs outside (16), the values which $\mu_{(0)}$ can take are constrained by

$$\mu_{(0)} \leq \frac{\sqrt{f_*} - 1}{A_{t*}}, \tag{33}$$

and the extraction process takes place in this region if $\mu_{(0)}$ is negative. Note that the change of sign in the inequality (33) is because $A_{t*} < 0$. Then, to maximize the range of $m_{(1)}$ the inequality (31) must be saturated; this occurs when the inequalities (32) or (33) are saturated, i.e., when $\mu_{(0)} \to (\sqrt{f_*} - 1)/A_{t*}$ to the left or to the right according to the sign of $\mu_{(0)}$. In this case, one can choose $m_{(1)} \to m_{(0)}$ thus maximizing the ratio $m_{(1)}/m_{(0)}$ that appears in (24). Then, the efficiency η of the Penrose process in the BM is bounded according to

$$\eta < \eta^b = -E^{min}_{(1)}(\rho_*, z_*). \tag{34}$$

The efficiency upper bound denoted by η^b is a function of $\mu_{(1)}$, the break-up point coordinates (ρ_*, z_*) and the BM parameters M_1, M_2 and R according to Eq. (26). The effect of varying each one of these parameters is analyzed in the next subsection.

B. Dependence of the maximum efficiency on the parameters.

From Eqs. (26) and (34) the explicit expression of the efficiency upper bound η^b is given by

$$\eta^b = \mu_{(1)}A_{t*} - \sqrt{f_*}. \tag{35}$$

The efficiency bound η^b has a linear dependence respect to the charge-mass ratio $\mu_{(1)}$. The dependence with respect to the break-up point coordinates (ρ_*, z_*) can be understood with the help of the energy levels shown in Fig. 3; the efficiency upper bound increases as the break-up point approaches one of the BHs, i.e., the Penrose process is more efficient if the break-up point is located near one of the horizons. If this is the case, using Eq. (1)the upper bound of efficiency for $\mu_{(1)} > 0$ is

$$\eta^b = \mu_{(1)}\sqrt{\frac{(R - M_1)^2 - M^2_2}{(R + M_1)^2 - M^2_2}} = -\mu_{(1)}\frac{M_2}{Q_2}, \tag{36}$$

and for $\mu_{(1)} < 0$ the upper bound is

$$\eta^b = -\mu_{(1)}\sqrt{\frac{(R - M_2)^2 - M^2_1}{(R + M_2)^2 - M^2_1}} = -\mu_{(1)}\frac{M_1}{Q_1}, \tag{37}$$

A relevant characteristic of the bound efficiency Eqs. (36) and (37) is that it depends on the charge-mass ratio $\mu_{(1)}$ that can be chosen arbitrarily large; even can be chosen such that the efficiency be greater than one, $\eta^b > 1$, as can occur in the case of one single charged BH [15, 17, 20] with charged particles that interact via electromagnetic forces with the BH.

From (35) we can identify two scenarios according to the sign of the charge-mass ratio μ, while the sign of A_t is defined by the break-up point coordinates. The break-up coordinates (ρ_*, z_*) dependence of η^b is illustrated in Fig. 6.a for several values of ρ_* and fixed values of M_1, M_2, R and $\mu_{(1)} < 0$. On the other hand, the dependence of the break-up coordinates for $\mu_{(1)} > 0$ is illustrated in Fig. 6.b. The negative efficiency implies that the particle that escapes towards infinity carries less energy than the incident particle. Note that the extraction process occurs only when the test particle and the BH have opposite charges.

Due to the fact that the upper bound of efficiency given in Eqs. (36) and (37) can be written in terms of the charges of the BHs that satisfy the relation $|Q_i| > M_i$, then the upper bound efficiency is less than $(-\mu_{(1)})$ for arbitrary M_1, M_2, and R, in contrast with the MP case analyzed in [21] where the upper bound is $(-\mu_{(1)})$. In the case that one of the BH masses is zero, the extraction process occurs if $\mu_{(1)}$ and the BH charge are oppositely charged and the maximum efficiency is $\eta^b = \pm\mu_{(1)}$, for Q_i negative and positive respectively.

To determine how the efficiency changes with BH masses, we analyze (35) in terms of the mass ratio $M_R = M_2/M_1$ with $M_2 < M_1$, total mass $M_T = M_1+M_2$ and fixed values of $\mu_{(1)}$ and $R = 1$, then $0 < M_R < 1$ and $0 < M_T < 1$. The dependence on the total mass M_T for a fixed value of mass ratio M_R, $\mu_{(1)}$ with different values of the break-up point is shown in Fig. 7. Note that in Fig. 7.a initially the efficiency for three selected break-up points is negative, this occurs because the break-up point is located outside the ergosphere and the total mass is small (therefore the ergosphere is small as well); for a fixed value of M_R the generalized ergosphere gets bigger as the total mass M_T increases until a critical value M_{Tcrit} is reached where the generalized ergosphere has its largest size and the upper bound efficiency is maximum. For $M_{Tcrit} < M_T$ the ergosphere gets smaller and the upper efficiency decreases even to the point of becoming negative.

The critical value of the total mass M_{Tcrit} is given by the M_T satisfying

$$\frac{d}{dM_T}\left(\eta^b\right) = 0, \quad \frac{d^2}{dM_T^2}\left(\eta^b\right) < 0, \tag{38}$$

where η^b is the efficiency upper bound given by Eq. (35), where the functions A_{t*} and f_* are rewritten in terms of total mass M_T and mass ratio M_R through the transformations $M_1 = M_T/(M_R+1)$ and $M_2 = M_R M_T/(M_R+1)$.

For $\mu_{(1)} > 0$ the ergosphere and upper bound efficiency exhibit the same qualitative behaviour, as shown in Fig. 8; the critical mass can be calculated with Eqs. (**??**).

Moreover, the mass ratio M_R for a fixed value of total mass $M_T = 1/2$ and a negative $\mu_{(1)}$, for different values of the break-up points is shown in Fig. 9. In this case the ergosphere and upper bound η^b decrease as M_R increases, i.e., the ergosphere and upper bound efficiency decrease when the masses M_1 and M_2 tend to be equal. The maximal efficiency upper bound η^b occurs when $M_R \to 0$, i.e., when $M_2 \to 0$ and is always less than or equal to $-\mu_{(1)}$. η^b as a function of M_R for $\mu_{(1)} > 0$ is shown in Fig. 10. In this case the upper bound η^b and ergosphere increase as M_R increases and the maximum upper bound for an arbitrary break-up point occurs when $M_R \to 1$.

C. Examples of the Penrose process

Once we have described the efficiency η^b, we will give some concrete examples of the Penrose process in a binary BH described by BM, whose efficiency approaches the theoretical maximum described by Eq. (36) for test particles with $\mu_{(1)} > 0$ and Eq. (37) for test particles with $\mu_{(1)} < 0$. First, we fix the values of M_1, M_2, and R. And then we fix the values of the charge mass ratio $\mu_{(1)}$ and the break-up point (ρ_*, z_*, ϕ_*), considered inside the generalized ergosphere. According to the analysis in Sec. IV A we set $m_{(0)} = 1$, $L_{(0)} = L_{(1)} = L_{(2)} = 0$, which means that all the trajectories are confined to the meridional plane $\phi = \phi_*$. The energy $E_{(1)}$ is determined by Eq. (26) and we set $E_{(0)} = 1$. The two scenarios for the process correspond to negative and positive charged test particle $\mu_{(1)}$; the charge mass ratio $\mu_{(0)}$ is bounded by two different limits depending where the break-up point (ρ_*, z_*) occurs according to Eqs. (32) and (33).

If the break-up point is located outside the region bounded by (16), then, according to Eqs. (30) and (33), we choose

$$\mu_{(0)} = \frac{\sqrt{f_*} - 1}{A_{t*}} - \epsilon_1, \tag{39}$$

$$m_{(1)} = 1 - \nu_1, \tag{40}$$

where ϵ_1 and ν_1 are small positive parameters. Substituting Eqs. (39) and (40) into Eq. (30), we find that ϵ_1, and ν_1, satisfy

$$\nu_1 > \frac{A_{t*}\epsilon_1}{\sqrt{f_*}}\left(\sqrt{1 - \frac{2\sqrt{f_*}}{A_{t*}\epsilon_1}} + 1\right). \tag{41}$$

On the other hand, if the break-up point occurs inside of the circle (16), then according to (30) and (32), we choose

$$\mu_{(0)} = \frac{\sqrt{f_*} - 1}{A_{t*}} + \epsilon_2, \tag{42}$$

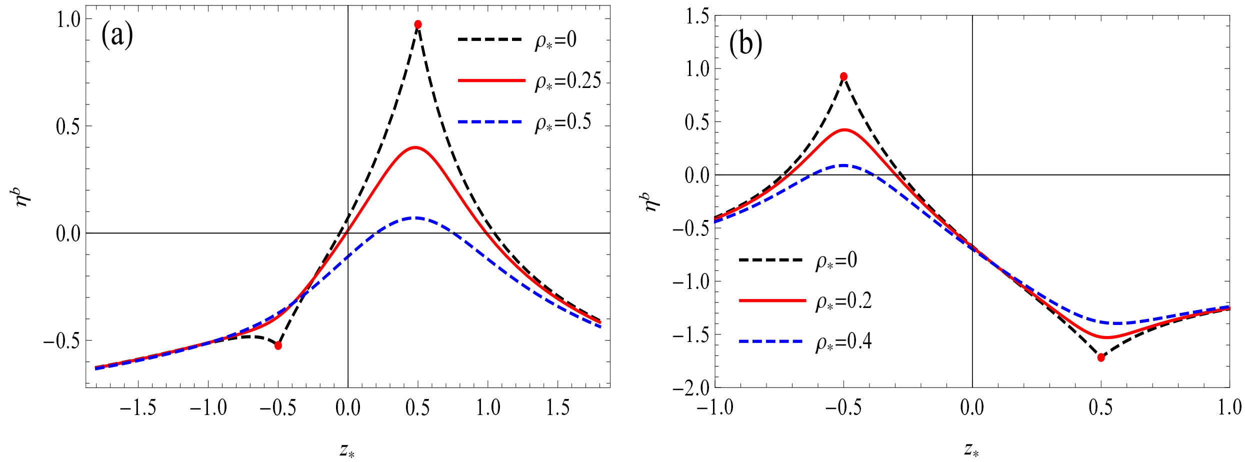

FIG. 6: It is illustrated the efficiency upper bound η^b as a function of z_* for fixed values of ρ_* and $M_1 = 0.5$, $M_2 = 0.2$, $R = 1$ and (a) $\mu_{(1)} = -1.7$, (b) $\mu_{(1)} = 3$.

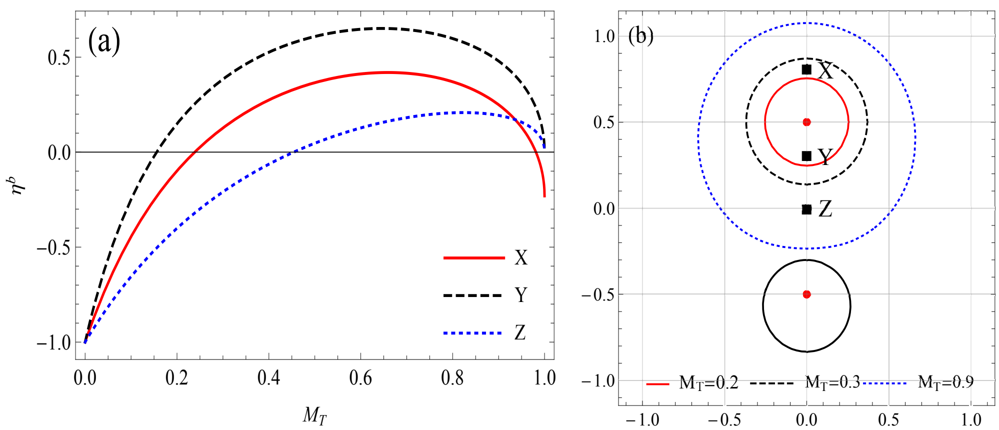

FIG. 7: It is shown the (a) Efficiency upper bound η^b as a function of $M_T = M_1 + M_2$ when $M_R = M_2/M_1 = 0.25$ and $\mu = -1.7$ for selected break-up points denoted by X, Y and Z. The values of M_{Tcrit} are $M_{Tcrit} = 0.658999$, $M_{Tcrit} = 0.645854$ and $M_{Tcrit} = 0.823573$ for the break-up points X, Y and Z, respectively. (b) Generalized ergospheres for selected values of M_T. The black square markers are the locations of the break-up points $(\rho_*, z_*) = (0, 0.8)$, $(\rho_*, z_*) = (0, 0.3)$ and $(\rho_*, z_*) = (0, 0)$ that are labeled as X, Y and Z, respectively. Each curve in (a) corresponds to one of the break-up points in (b). The dots represent the BHs.

$$m_{(1)} = 1 - \nu_2, \tag{43}$$

Substituting these expressions into (30), we find that ϵ_2 and ν_2 satisfy

$$\nu_2 > \frac{A_{t*}\epsilon_2}{\sqrt{f_*}}\left(\sqrt{1 + \frac{2\sqrt{f_*}}{A_{t*}\epsilon_2}} - 1\right), \tag{44}$$

the charge mass ratio $\mu_{(2)}$ and energy per unit mass $E_{(2)}$ can be determined from Eqs. (18) and (20).

For a given angle between the velocities, $\theta_{(0)} = \arg(\dot\rho_{(0)} + i\dot z_{(0)})$, Eqs. (45) and (46) can be used to determine $\dot\rho_{(0)}$ and $\dot z_{(0)}$ at the break-up point.

At the break-up point, according to (25), we have $\dot\rho_{(1)} = \dot z_{(1)} = 0$ for the negative energy fragment. For the incident particle, if the break-up point is outside the circular region (16) and $E_{(0)} = 1$ then

$$\dot\rho_{(0)}^2 + \dot z_{(0)}^2 = \frac{\left(1 + A_{t*}(1-\epsilon_1)\right)^2}{e^{2\gamma_*}} - \frac{f_*}{e^{2\gamma_*}}, \tag{45}$$

while if the break-up point is inside (16) we have,

$$\dot\rho_{(0)}^2 + \dot z_{(0)}^2 = \frac{\left(1 + A_{t*}(1+\epsilon_2)\right)^2}{e^{2\gamma_*}} - \frac{f_*}{e^{2\gamma_*}}. \tag{46}$$

The values for $\dot\rho_{(2)}$ and $\dot z_{(2)}$ are obtained from linear momentum conservation (21). With this setting of parameters the trajectories $T_{(0)}$, $T_{(1)}$ and $T_{(2)}$ are completely determined and the efficiency of the Penrose process is given by $\eta_{1,2} = (1-\nu_{1,2})\eta^b$. In order to maximize the efficiency we need to choose $\nu_{1,2}$ as small as possible. However, $\epsilon_{1,2}$ and $\nu_{1,2}$ cannot be zero because the

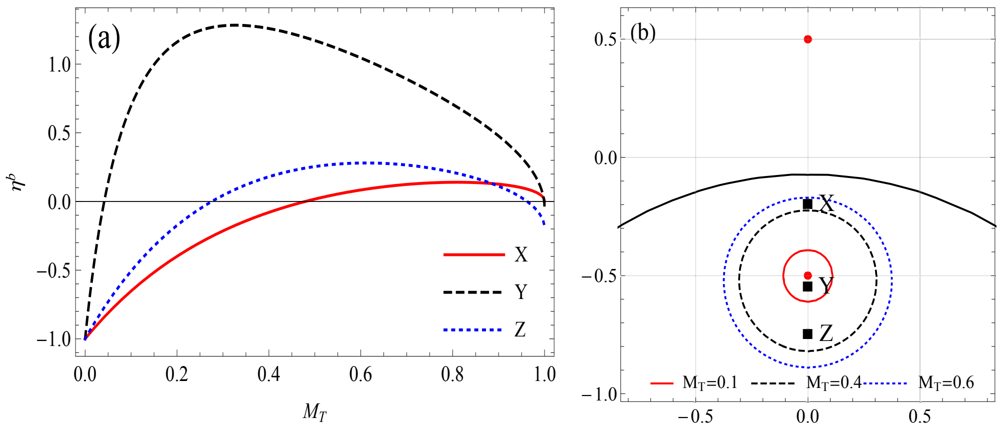

FIG. 8: It is shown the (a) Efficiency upper bound η^b as a function of M_T when $M_R = 0.75$ and $\mu = 3$ for selected break-up points. The values of M_{Tcrit} are $M_{Tcrit} = 0.809496$, $M_{Tcrit} = 0.326936$ and $M_{Tcrit} = 0.611923$ for the break-up points X, Y and Z, respectively. (b) Generalized ergospheres for selected values of M_T. The square markers are the locations of the break-up points $(\rho_*, z_*) = (0, -0.2)$, $(\rho_*, z_*) = (0, -0.55)$ and $(\rho_*, z_*) = (0, -0.75)$ that are labeled X, Y and Z respectively. The dots represent the BHs. Each curve in (a) corresponds to one of the break-up points in (b).

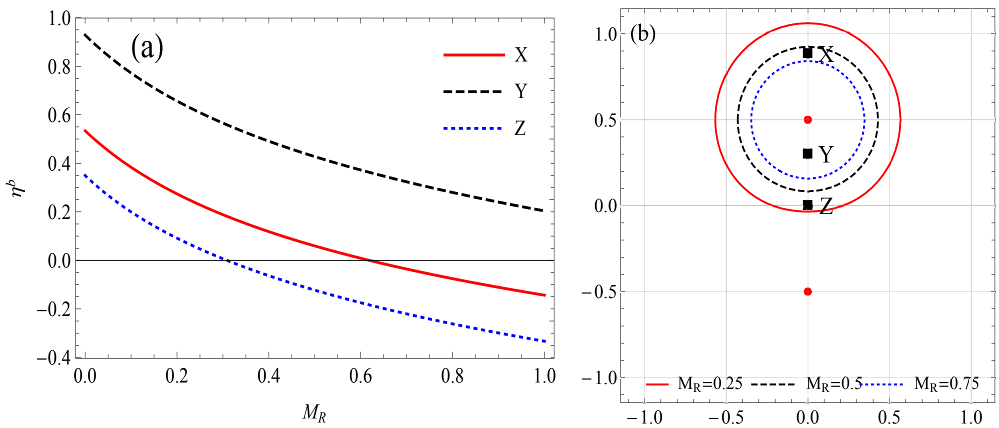

FIG. 9: It is plotted the (a) Efficiency upper bound η^b as a function of M_R when $M_T = 0.5$ and $\mu = -1.7$ for selected break-up points. (b) Generalized ergospheres for selected values of M_R. The square markers are the locations of the break-up points $(\rho_*, z_*) = (0, 0.88)$, $(\rho_*, z_*) = (0, 0.3)$ and $(\rho_*, z_*) = (0, 0)$ that are labeled X, Y and Z, respectively. The dots represent the BHs. Each curve in (a) corresponds to one of the break-up points in (b).

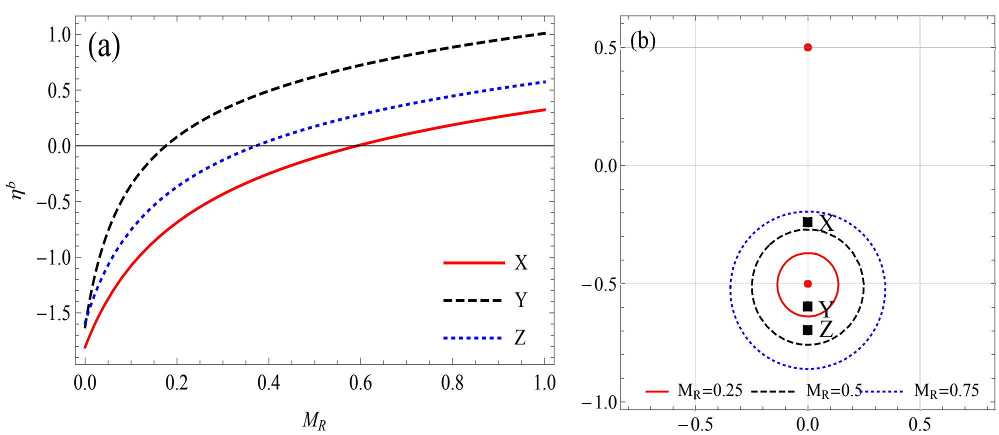

FIG. 10: It is illustrated the (a) Efficiency upper bound η^b as a function of M_R when $M_T = 0.5$ and $\mu = 3$ for selected break-up points. (b) Generalized ergospheres for selected values of M_R. The square markers are the locations of the break-up points $(\rho_*, z_*) = (0, -0.24)$, $(\rho_*, z_*) = (0, -0.6)$ and $(\rho_*, z_*) = (0, -0.7)$ that are labeled X, Y and Z respectively. The dots represent the BHs. Each curve in (a) corresponds to one of the break-up points in (b).

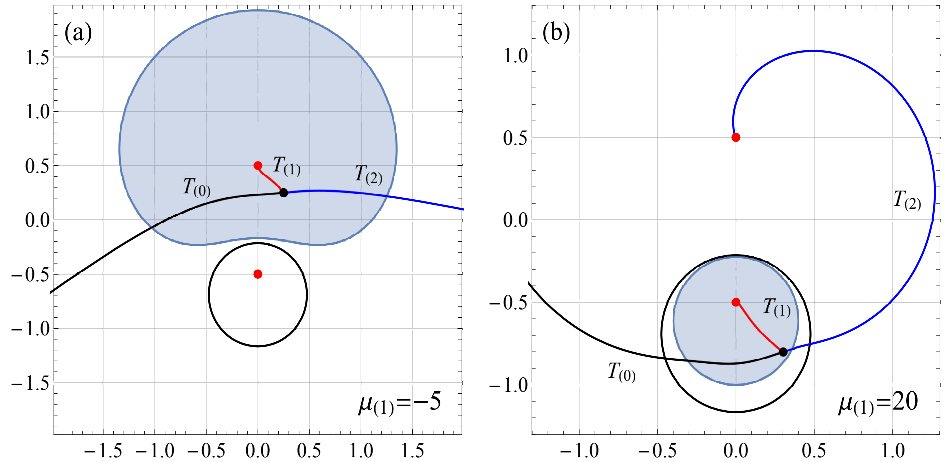

FIG. 11: Examples of Penrose's processes near the maximum theoretical efficiency in a BM spacetime. The efficiencies of the processes are 90% of the theoretical maximum. In both panels the incoming trajectory $T_{(0)}$ (black curve) splits at the black point into the negative energy trajectory $T_{(1)}$ (red curve) and the trajectory of the particle that escapes $T_{(2)}$. The Bonnor parameters in both cases are fixed as $M_1 = 0.5$, $M_2 = 0.2$, $R = 1$, the parameter ν and ϵ are fixed as $\nu_{1,2} = 10^{-2}$, $\epsilon_{1,2} = 10^{-5}$, the charge-mass ratio, the break-up point and the angle $\theta(0)$ are fixed as: (a) $\mu_{(1)} = -5$, $(\rho_*, z_*) = (1/4, 1/4)$ and $\theta_{(0)} = 0.0872665$; (b) $\mu_{(1)} = 20$, $(\rho_*, z_*) = (0.3, -0.8)$ and $\theta_{(0)} = 0.296706$. The initial values of the parameters that generate these trajectories are shown in Tables I and II. The respective efficiency upper bound is $\eta^b = 1.20854$ (left panel) and $\eta^b = 0.208203$ (right panel).

inequalities (41) or (44) cannot be saturated; but it is possible, in principle, to set infinitesimally small values for $\epsilon_{1,2}$ and $\nu_{1,2}$. According to these considerations we explore two specific examples where the efficiency corresponds to 90% for a break-up point located outside and inside of the region bounded by (16) resulting that the extraction process occurs with the BH with positive or negative charge, respectively.

TABLE I: Initial values that generate the trajectories $T_{(0)}$, $T_{(1)}$ and $T_{(2)}$ in the Penrose process shown in Fig. 11.a. The derivatives $\dot{\rho}_{(i)}$ and $\dot{z}_{(i)}$ are evaluated at the break-up point.

i	$m_{(i)}$	$\mu_{(i)}$	$E_{(i)}$	$L_{(i)}$	$\dot{\rho}_{(i)}$	$\dot{z}_{(i)}$
0	1	2.70371	1	0	1.45015	0.126872
1	0.9	-5	-1.20854	0	0	0
2	0.0998852	72.1199	20.9008	0	14.5182	1.27018

TABLE II: Initial values that generate the trajectories $T_{(0)}$, $T_{(1)}$ and $T_{(2)}$ in the Penrose process shown in Fig. 11.b. The derivatives $\dot{\rho}_{(i)}$ and $\dot{z}_{(i)}$ are evaluated at the break-up point.

i	$m_{(i)}$	$\mu_{(i)}$	$E_{(i)}$	$L_{(i)}$	$\dot{\rho}_{(i)}$	$\dot{z}_{(i)}$
0	1	2.70371	1	0	1.45015	0.126872
1	0.9	-5	-1.20854	0	0	0
2	0.0998852	72.1199	20.9008	0	14.5182	1.27018

Fig. 11.a shows the Penrose extraction from a BH with negative charge. The BM parameters M_1, M_2, and R are fixed. It corresponds to the extraction process where the break-up point occurs outside (16) and the charge-mass ratio of the negative energy fragment (red line) is negative $\mu_{(1)}$ (e. g. Fig. 2.c), the setting of these parameters enables us to determine the trajectories $T_{(1)}$, having in mind that the energy $E_{(1)}$ associated to the trajectory $T_{(1)}$, Eq. (14), is the minimum possible and the trajectories $T_{(0)}$ and $T_{(2)}$ are fully described once we fix $\nu_{1,2}$, $\epsilon_{1,2}$, and $\theta_{(0)}$. On the other hand, in Fig. 11.b it is shown the Penrose process where the break-up point occurs inside the region bounded by (16) for a negatively charged particle. We can highlight two different features of the Penrose process in the BM binary BH in contrast with the MP binary: first, the process of extraction can occur for positively charged test particles with the negatively charged BH. Second, if the Penrose process occurs in the BH with negative charge, the particle that escapes with more energy can be trapped by the other BH as shown in Fig. 11.b. The parameters that generate these examples satisfy the conservations Eqs. (18)-(23) and are given in Tables I and II.

V. CONCLUSIONS

We have analyzed in detail the possibility of energy extraction from the Bonnor BH binary (BM), that describes two oppositely charged BH kept apart by a strut [25, 26]. In contrast to the Majumdar-Papapetrou (MP) setup, the BH charges do not balance the gravitational attraction.

We determine a generalized ergosphere that depends on the parameters of the BM and the charge-mass ratio μ of the test particle and we showed that energy extraction is possible; the sign of the electric potential A_t is defined by the location where it is evaluated. As a first difference with the MP case the generalized ergosphere exists for positive and negatively charged test particles μ. Another remarkable difference with respect to the MP case is that the ergosphere cannot include both BHs, but only one; the ergosphere encloses the BH with charge opposite to the one of the test particle. Initial conditions of the particle trajectory can be found such that the particle that escapes with more energy is trapped by the other BH. We have studied the efficiency of the process and its dependence on the break-up point location. We determined as well the total mass $M_T = M_1 + M_2$ and mass ratio $M_R = M_2/M_1$ that renders the highest efficiency η^b. The upper bound efficiency in the BM is always lower compared to the MP efficiency [21]. The behavior of η^b as a function of M_R depends on the sign of μ. If $\mu < 0$ then η^b decreases when $M_R \to 1$; while if $\mu > 0$ then η^b increases when M_R approaches 1. Moreover the maximum efficiency η^b does not increases monotonically as M_T increases, but there is a certain M_{Tcrit} such that for $M_T > M_{Tcrit}$, η^b decreases, and even can reach negative values.

Due to the vast recent observations reported by the LIGO-Virgo Collaboration, so far it has been able to identify multiple candidates for compact binary systems. We believe that the study of the Penrose process in BM is useful because it extends the analysis carried out for a MP black hole in [21] and this phenomenon could give us relevant information regarding other astrophysical aspects such as the superradiant effects [32–34] where some earlier researches have proposed that compact binary systems are intimately related to this effect [36, 37]. Moreover, the magnetic variant of the Penrose process that takes into account the combined influence of external magnetic field and the rotation of a BH seems to be connected to the origin of accretion disks where the energy extraction into jets can befall, or even yet the generation of ultra-high energy cosmic rays [8, 35]. In this direction we aim to develop further research of the magnetic Penrose process in BH binaries.

VI. ACKNOWLEDGMENTS

This work has been supported by CONACyT Grant No. 284498. ICM acknowledges the financial support of SNI-CONACyT, México, grant with CVU No. 173252. AB acknowledges the financial support of CONACyT, México, through the PhD Scholarship with CVU No. 933515.

---

[1] R. P. Kerr, Gravitational Field of a Spinning Mass as an Example of Algebraically Special Metrics, Phys. Rev. Lett. **11**, 237 (1963).

[2] M. Visser, The Kerr spacetime: A Brief introduction, in Kerr Fest: Black Holes in Astrophysics, General Relativity and Quantum Gravity (2007) arXiv:0706.0622.

[3] S. A. Teukolsky, The Kerr metric, Class. Quantum Grav. **32**, 124006 (2015).

[4] R. Penrose and R. M. Floyd, Extraction of Rotational Energy from a Black Hole, Nat. Phys. Sci. **229**, 177 (1971).

[5] G. Denardo and R. Ruffini, On the energetics of Reissner Nordström geometries, Phys. Lett. B **45**, 259 (1973).

[6] D. Christodoulou, Reversible Transformations of a Charged Black Hole, Phys. Rev. D **4**, 3552 (1971).

[7] J. Schnittman, The collisional Penrose process, Gen. Relativ. Gravit. **50**, 77 (2018).

[8] Z. Stuchlík, M. Kološ, and A. Tursunov, Penrose process: Its variants and astrophysical applications, Universe **7** (2021).

[9] N. Dadhich, A. Tursunov, B. Ahmedov, and Z. Stuchlík, The distinguishing signature of magnetic Penrose process, Mon. Not. Roy. Astron. Soc. **478**, L89 (2018).

[10] Z. Stuchlík, M. Kološ, and A. Tursunov, Possible signature of the magnetic fields related to quasi-periodic oscillations observed in microquasars, Eur. Phys. J. C **77**, 860 (2017).

[11] M. Kološ, Z. Stuchlík, and A. Tursunov, Quasiharmonic oscillatory motion of charged particles around a Schwarzschild black hole immersed in a uniform magnetic field, Classical and Quantum Gravity **32**, 165009 (2015).

[12] M. Kološ, Z. Stuchlík, and A. Tursunov, Radiative penrose process: Energy gain by a single radiating charged particle in the ergosphere of rotating black hole, Phys. Rev. D **103**, 024021 (2021).

[13] M. Kološ, Z. Stuchlík, and A. Tursunov, Light escape cones in local reference frames of kerr-de sitter black hole spacetimes and related black hole shadows, Eur. Phys. J. C **78**, 180 (2018).

[14] K. Parfrey, A. Philippov, and B. Cerutti, First-Principles Plasma Simulations of Black-Hole Jet Launching, Phys. Rev. Lett. **122**, 035101 (2019).

[15] M. Bhat, S. Dhurandhar, and N. Dadhich, Energetics of the Kerr-Newman black hole by the penrose process, J. Astrophys. Astron. **6**, 85 (1985).

[16] A. Tursunov, B. Juraev, Z. Stuchlík, and M. Kološ, Electric Penrose process: High-energy acceleration of ionized particles by nonrotating weakly charged black hole, Phys. Rev. D **104**, 084099 (2021).

[17] S. Parthasarathy, S. M. Wagh, S. V. Dhurandhar, and N. Dadhich, High Efficiency of the Penrose Process of Energy Extraction from Rotating Black Holes Immersed in Electromagnetic Fields, Astrophys. J. **307**, 38 (1986).

[18] S. M. Wagh, S. V. Dhurandhar, and N. Dadhich, Revival of the Penrose Process for Astrophysical Applications, Astrophys. J. **290**, 12 (1985).

[19] S. M. Wagh and N. Dadhich, The energetics of black holes in electromagnetic fields by the penrose process, Phys. Rept. **183**, 137 (1989).

[20] S. Shaymatov, P. Sheoran, R. Becerril, U. Nucamendi, and B. Ahmedov, Efficiency of Penrose process in spacetime of axially symmetric magnetized Reissner-Nordström black hole, Phys. Rev. D **106**, 024039 (2022).

[21] L. T. Sanches and M. Richartz, Energy extraction from non-coalescing black hole binaries, Phys. Rev. D **104**,

(2021).
[22] S. D. Majumdar, A class of exact solutions of Einstein's field equations, Phys. Rev. **72**, 390 (1947).
[23] A. Papapetrou, A static solution of the equations of the gravitational field for an arbitrary charge distribution, Proc. R. Irish Acad., Sect. A **51**, 191 (1947).
[24] J. B. Hartle and S. W. Hawking, Solutions of the Einstein-Maxwell equations with many black holes, Commun. Math. Phys. **26**, 87 (1972).
[25] W. B. Bonnor, A three-parameter solution of the static Einstein-Maxwell equations, J. Phys. A Math Gen. **12**, 853 (1979).
[26] I. Cabrera-Munguia, V. S. Manko, and E. Ruiz, A combined Majumdar-Papapetrou-Bonnor field as extreme limit of the double-Reissner-Nordström solution, Gen. Relativ. Gravit. **43**, 1593 (2011).
[27] R. Bach and H. Weyl, Neue Lösungen der Einsteinschen Gravitationsleichungen, Math. Z. **13**, 134 (1922).
[28] W. Israel, Line sources in general relativity, Phys. Rev. D **15**, 935 (1977).
[29] V. S. Manko, Double-Reissner-Nordström solution and the interaction force between two spherical charged masses in general relativity, Phys. Rev. D **76**, 124032 (2007).
[30] I. Cabrera-Munguia and A. Macías, On naked singularities in the extreme double Reissner-Nordström solution, in AIP Conf. Proc., Vol. **1577** (AIP Publishing LLC, 2014).
[31] F. Dubeibe and José D. Sanabria-Gómez, Geodesic motion in a stationary dihole spacetime, Phys. Rev. D **94**, 044058 (2016).
[32] C. Misner, Stability of Kerr black holes against scalar perturbations, Bull. Amer. Phys. Soc. **17**, 472 (1972).
[33] Jacob D. Bekenstein, Extraction of Energy and Charge from a Black Hole, Phys. Rev. D **7**, 949–953 (1973).
[34] R. Brito, V. Cardoso and P. Pani, Superradiance, Lect. Notes Phys. **906**, 1 (2015).
[35] A. Tursunov, Z. Stuchlík, M. Kološ, N. Dadhich and B. Ahmedov, Supermassive Black Holes as Possible Sources of Ultrahigh-energy Cosmic Rays, Astrophys. J. **985**, 14 (2020).
[36] J. G. Rosa, Testing black hole superradiance with pulsar companions, Phys. Lett. B **749**, 226 (2015).
[37] L. K. Wong, Superradiant scattering by a black hole binary, Phys. Rev. D **100**, 044051 (2019).